Copying a Plasmonic Signal From an Optical Signal
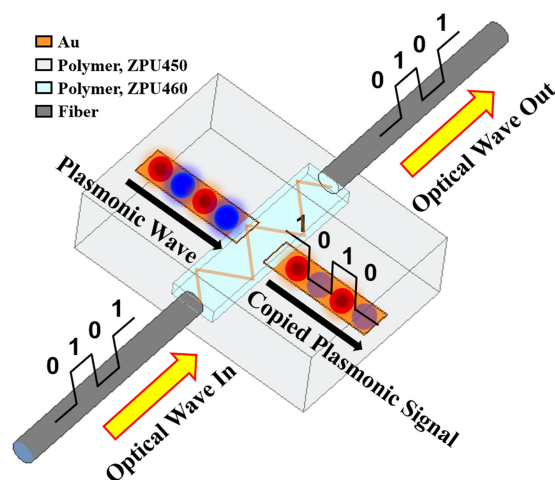
Sung-Ryoung Koo
Guhwan Kim
Dong Hun Lee
Kyung-Jo Kim
Myung-Hyun Lee

Copying a Plasmonic Signal From an Optical Signal

Sung-Ryoung Koo [ID],[1] **Guhwan Kim** [ID],[1] **Dong Hun Lee** [ID],[1]
Kyung-Jo Kim [ID],[2] **and Myung-Hyun Lee** [ID] [1]

[1]Department of Electrical and Computer Engineering, Sungkyunkwan University, Suwon
16419, Korea
[2]College of Optical Sciences, University of Arizona, Tucson, AZ 85721 USA

Abstract: We propose a plasmonic signal copier (PSC) composed of a gapped surface
plasmon polariton waveguide (SPPW) and an optical waveguide laid across the gap. The
interaction between an SPP and an optical signal around the gap edge is demonstrated
experimentally and numerically with polarizations of the incident optical wave. A plas-
monic signal is invertedly copied from a TE-polarized optical signal incident to the optical
waveguide. The symmetrically distributed charges induced from the TE-polarized optical
waves on the metal gap edges of input/output SPPWs were determined to be an essential
trigger of the copied plasmonic signal. The characteristics of the PSC enable creation of a
plasmonic-based circuit system that is compatible with an optical-based circuit system.

Index Terms: Plasmonics, surface plasmon polariton (SPP), waveguide devices, plasmonic
signal, optical signal.

1. Introduction

Electronic circuits provide the ability to control the transport and storage of electrons. However,
it is difficult to further increase the signal processing speed of electronic circuits, mainly due to
RC delay issues in electronic devices. Photonics offers an effective solution to this problem by
implementing optical signal processing circuits [1]–[6]. However, the micro-scaled components of
photonics have limited their integration due to the diffraction limit of light in optical devices [7].
Plasmonics is introduced to solve problems related to the operating speed limitation in electronics
and the dimension limitation in photonics at the same time [8]–[14].

Photonics allows high-performance computing (HPC) by introducing a photonic plane in a next-
generation 3D CMOS chip [3]–[6]. HPC requires very high clock speeds and data transfer rates
with very low power consumption. Owing to the size problems caused by the diffraction limit of light
[7], low-power operation in photonics has limitations. An alternative plasmonic plane can solve this
problem by introducing nano-scaled surface plasmon polariton (SPP) waveguides into the signal
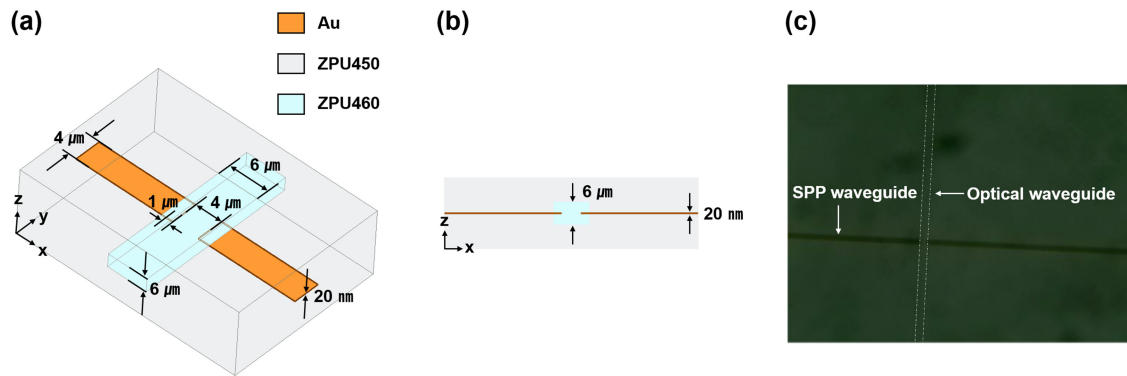processing plane in next-generation 3D CMOS chips [12]–[14].

Fig. 1. (a) Schematic view of the PSC. (b) Cross-section view of the PSC in the xz-plane. (c) Optical micrograph of the 4-μm-wide input and output SPP waveguides with a 4-μm gap length for the G-SPPW and the 6×6 μm^2 optical waveguide.

Photonic systems in ultra-high-speed signal processors are pervasive and should be even more so in the future, even though they have some limitations. Therefore, the introduced plasmonic systems must be compatible with micro-scaled photonic systems in terms of signal and size. Micro-scaled photonic signals can excite a micro-scaled plasmonic signal directly, with high efficiency; however, they cannot excite a nano-scaled surface plasmonic signal. A mode size converter from a micro-scaled plasmonic signal to a nano-scaled plasmonic signal has been demonstrated [15],[16]. Using this converter is the best way to provide compatibility with optical signals, which excite micro-scaled plasmonic signals.

Gapped SPP waveguides (G-SPPWs) were suggested and tested numerically and experimentally in terms of propagation and coupling losses [17]–[20]. In this work, we propose a plasmonic signal copier (PSC) using a G-SPPW and an optical dielectric channel waveguide laid across the gap. The PSC gains compatibility with optical systems by generating an invertedly copied plasmonic signal. The experimental analysis is presented in Section 2, and the results and discussion with numerical analysis using the FDTD method are given in Section 3. Finally, the concluding remarks are summarized in Section 4.

2. Experimental Analysis

2.1. Design of the PSC

The PSC is composed of a G-SPPW and an optical dielectric channel waveguide laid across the gap, as shown in Fig. 1. Fig. 1(a) and (b) show the schematic view and the cross-section view in xz-plane of the PSC, respectively. Fig. 1(c) shows the optical micrograph of the PSC. The white dotted lines in Fig. 1(c) indicate the optical dielectric channel waveguide laid across the gap. The thicknesses of the input and output SPP waveguides (SPPWs), clad and core in the optical waveguide were fixed at 20 nm, 100 μm, and 6 μm, respectively. The widths of the SPP and optical waveguides were 4 μm and 6 μm, respectively. The gap length in the G-SPPW was 4 μm. The gap edges of input/output SPPWs were overlapped by 1 μm on both sides. Gold was used as a metal strip material, and low-loss polymers were used as dielectric materials. The refractive indices of the gold, dielectric for the core, and dielectric for the 50-μm-thick upper and lower cladding layers were 0.550-11.4912i, 1.460, and 1.450, respectively, at a wavelength of 1.550 μm [21], [22].

2.2. Fabrication of the PSC

The evaporated gold strip of the G-SPPW was surrounded by polymers in the PSC. The polymers were ultraviolet (UV)-curable epoxies, i.e., ZPU460 and ZPU450 for the optical waveguide and
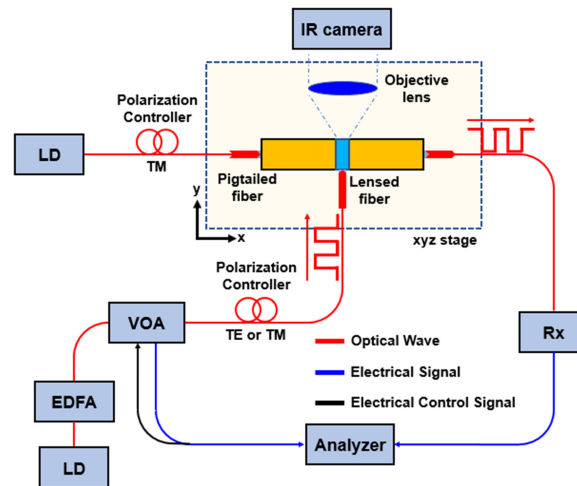
Fig. 2. Experimental setup for PSC measurement.

clad, respectively, supplied by Chemoptics Inc., Korea. For convenience, we divided the polymers into lower and upper layers of the same materials for the 6-μm-thick cored optical waveguide. For the lower layer, ZPU450 (50-μm–thick) was spin-coated on a 4-inch Si wafer and then cured with UV light in a nitrogen atmosphere. For the 6-μm-thick cored optical waveguide laid across the gap, ZPU460 (3-μm–thick) was spin-coated and patterned via photolithography and ICP etching. Again, ZPU450 (3-μm–thick) was spin-coated and cured. Gold strips (20-nm–thick) were thermally evaporated, followed by a lift-off photolithography process. For the upper layer, ZPU460 (3-μm-thick) was again spin-coated, and the 6×6 μm^2 core was patterned onto that. Lastly, ZPU450 (50-μm–thick) was spin-coated and cured. For ease of measurement, the 1-cm-long PSC chip was pigtailed with polarization-maintaining single-mode-fibers (PMSMFs) at the input and the output of the G-SPPW. The detailed fabrication process is explained in ref [23].

2.3. Measurement of the PSC

Fig. 2 shows the experimental setup for PSC measurement. A continuous plasmonic wave was excited using a 1.550-μm laser diode (LD) and a polarization controller for the TM-polarized light. An optical wave from the other 1.550-μm LD was amplified using an erbium-doped fiber amplifier (EDFA) and modulated with a variable optical attenuator (VOA) controlled with an electric signal from a function generator. The modulated optical signal was incident to the optical waveguide laid across the gap of G-SPPW with a TE- or TM-polarized state using a polarization controller and a lensed fiber. The electric(magnetic) field of TE(TM)-polarized state is parallel to the planar plane in the PSC chip. To test the interaction with an SPP and the polarized optical modes around the gap edge, we measured the output SPP signal at the end of the output SPPW of the G-SPPW.

3. Results and Discussion

Fig. 3 shows the output SPP signal after interaction around the gap edges with the input SPP and the TM- or TE-polarized optical wave with the modulated signal. The output SPP signal was not copied with the input optical signal modulated in the TM-polarized optical wave, as shown in Fig. 3(a). However, the output SPP signal was invertedly copied with the input optical signal modulated in the TE-polarized optical wave, as shown in Fig. 3(b). The copied plasmonic signal was dependent on polarization of the optical wave that enters the optical dielectric channel waveguide. The pigtailed 1-cm long PSC sample has a 4-μm gap length, 4-μm-wide SPP waveguides, and 6×6 μm^2 optical dielectric channel waveguide with a 1-μm overlap in the gap at both sides, as
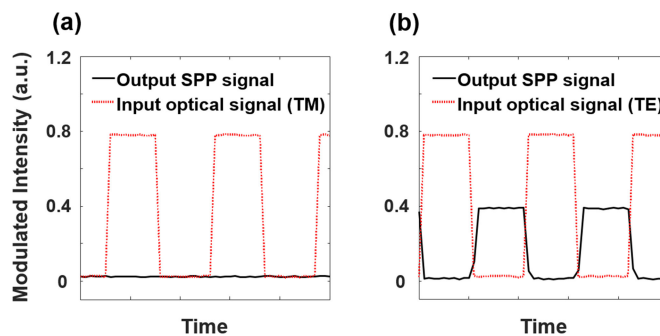
Fig. 3. Measured output plasmonic signals with regard to polarization of the input optical wave: (a) input TM-polarized optical signal and (b) input TE-polarized optical signal. The input optical wave was modulated at 3 Hz frequency.

shown in Fig. 1(a). The LD power for excitation of the input SPP was 1 dBm, and the power of the input optical wave was 21 dBm. The modulation frequency in the input optical wave was 3 Hz. The invertedly copied SPP output signal was obtained with only the modulated TE-polarized optical signal when the power of the input optical wave was greater than 15 dBm. This is mainly due to the small overlapped region between the edge surface of SPPWs and the optical mode in the dielectric channel waveguide as shown in Fig. 1(b). There was no copied SPP output signal with the modulated TM-polarized optical signal (Fig. 3(a)).

SPPs were also induced and propagate in the y-direction, as in Fig. 1(a), around the gap edges via excitation of the input TM- or TE-polarized optical wave in the optical waveguide. To distinguish the SPP excited from the input LD in the G-SPPW and the SPPs excited from the input TM- or TE-polarized optical wave around the gap edges, SPPs will be referred to as the SPP, TM-induced SPP, and TE-induced SPP, respectively. The differences in optical characteristics of the SPP, TM-induced SPP, and TE-induced SPP around the gap edges were numerically investigated using the FDTD method with interaction of the SPP and the input TM- or TE-polarized optical wave.

The characteristics of the SPP and TM-induced SPP are similar since they are excited with incident TM-polarized optical waves. However, the TE-induced SPP around the gap edges has different properties. To define the electric (E) field transition that induces fluctuation of free electrons inside the metal, the divergence equation of the E field in Maxwell's equations was used. Divergence of the E field was calculated about the SPP, TM-induced SPP, and TE-induced SPP around the gap edge inside the metal in the vertical (z) direction. In simulations, the metal strip was on the xy-plane, and the SPP propagated in the x-direction. The width and thickness of the SPP waveguide were 4 μm (from -2 μm to $+2$ μm) in the y-direction and 20 nm (from -10 nm to $+10$ nm) in the z-direction, respectively. The gap length is 4 μm (from 0 μm to $+4$ μm) in the x-direction, and the output SPPW in the G-SPPW started at $+4$ μm in the x-direction. Divergence of the E field was calculated around the gap edge of the output SPPWs. Based on the center of the metal strip around the gap edge, the SPP and TM-induced SPP had asymmetric characteristics (Figs. 4(a, b)), but the TE-induced SPP was symmetric in terms of divergence of the E field (Fig. 4(c)). Charge densities (ρ_v) of free electrons inthe SPP, TM-induced SPP, and TE-induced SPP were calculated from the divergence equation of the E field at the output SPPW in each propagation direction. Fig. 5 shows the surface ρ_v distribution on the top and bottom surfaces with different propagation directions of the SPP, TM-induced SPP, and TE-induced SPP. The SPP propagating in the x-direction of the output SPPW was coupled with asymmetrically distributed ρ_v with respect to the metal center in the z-direction (Fig. 5(a)). As expected, the TM-induced SPP propagating in the y-direction around the gap edges was coupled with the asymmetrically distributed ρ_v (Fig. 5(b)). Alternatively, the TE-induced SPP propagating in the y-direction around the gap edge was coupled with the symmetrically distributed ρ_v (Fig. 5(c)).
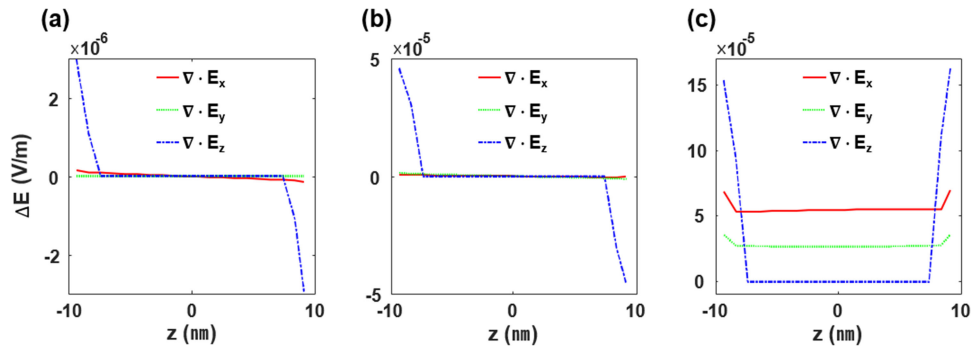
Fig. 4. Simulated divergence of the electric field with regard to SPP and polarization-induced SPPs around the gap edge: (a) the SPP, (b) the TM-induced SPP, and (c) the TE-induced SPP.
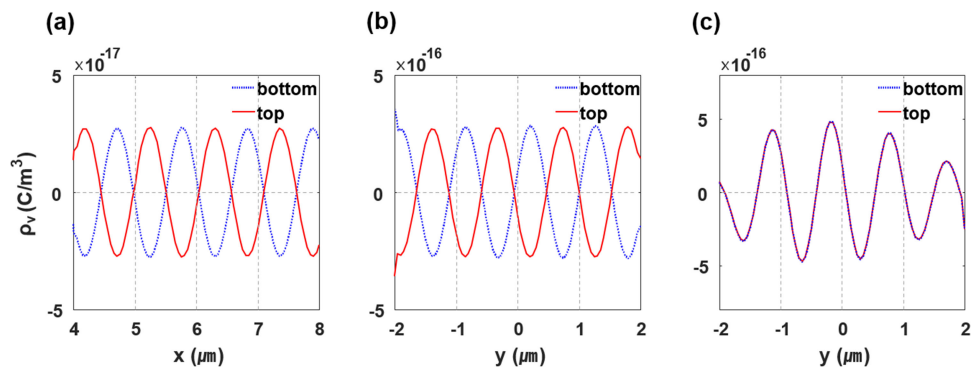

Fig. 5. Simulated top/bottom surface charge density (ρ_v) with regard to SPP and polarization-induced SPP in each propagation direction: (a) the ρ_v of the SPP, (b) the ρ_v of the TM-induced SPP, and (c) the ρ_v of the TE-induced SPP.

When the SPP propagated simultaneously with the polarization-induced SPPs around the gap edges, the charges fluctuated in different distributions depending on polarization of the optical wave incident to the optical waveguide. The SPP intersecting with the TM-induced SPP around the gap edges was coupled with asymmetrically distributed charges. The sinusoidal wave form of the charge oscillation in the SPP (Fig. 5(a)) coupled with the TM-induced SPP was maintained and not perturbed around the gap edge, as shown in Fig. 6(a). However, the SPP intersecting with the TE-induced SPP was coupled with symmetric-like distributed charges from 4 μm to 7 μm in the x-direction of the output SPPW (Fig. 6(b)). Insets in Fig. 6 show absolute magnitudes of charge density ($|\rho_v|$) with an enlarged y-axis scale (using the same x-axis scale). The inset in Fig. 6(a) shows that the $|\rho_v|$ values on the bottom and top surfaces were the same. In the asymmetric region, particularly after ~7 μm in Fig. 6(b), the $|\rho_v|$ values on the bottom and top surfaces were different from when the SPP intersected with the TM-induced SPP (Fig. 6(a)). Based on the simulation in Fig. 6, it is speculated that the SPP was perturbed with the TE-induced SPP around the gap edge. The perturbed SPP combined with the symmetric-like charge distribution could have a high absorption loss [24]. Therefore, the ON/OFF state of the TM-polarized optical signal incident to the optical waveguide cannot disturb the SPP around the gap edges. However, when the TE-polarized optical signal is incident to the optical waveguide, the SPP can be perturbed and disturbed by the TE-induced SPP around the gap edges in the ON state of the signal. In the OFF state of the TE-polarized optical signal, the SPP excites light in the gap edge of the input SPPW, and the light in the gap again excites the SPP without any perturbed state in the gap edge of the
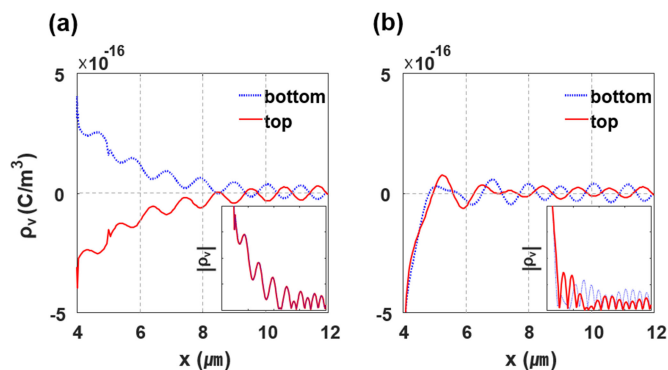
Fig. 6. Simulated top/bottom surface charge density (ρv) values of the SPP intersecting coincidently with the polarization-induced SPPs: (a) the ρv of the SPP intersecting coincidently with the TM-induced SPP and (b) the ρv of the SPP intersecting coincidently with the TE-induced SPP. The insets show the absolute magnitude (|ρv|) of the charge density.

output SPPW. Consequently, the symmetrically distributed charges from the TE-induced SPP are an essential trigger of the copied plasmonic signal. The SPP can be controlled to be the inverted copied SPP signal based on the ON/OFF state of the TE-polarized optical wave around the gap edges overlapped with the optical waveguide.

After generating the copied plasmonic signal from the interaction with the SPP and the optical signals, the used optical signals could be re-used in another optical-based circuit system. Thus, the PSC has compatibility with another optical-based circuit system.

4. Conclusion

We propose the concept of a PSC and analyze it experimentally and numerically. The PSC generates a plasmonic signal invertedly from an optical signal. The SPP signal is copied from only the TE-polarized optical wave with a modulated input optical signal. The symmetrically distributed charge from the TE-induced SPP around the metal gap edge is determined to be an essential trigger of the copied plasmonic signal. The SPP can be controlled by the ON/OFF state of the TE-polarized optical signal on the PSC. The presented PSC can be a useful plasmonic device for generating a plasmonic signal that has compatibility with an optical-based circuit system.

References

[1] M. J. Kobrinsky *et al.*, "On-chip optical interconnects," *Intel Tech. J.*, vol. 8, no. 2, pp. 129–141, 2004.
[2] D. Thomson *et al.*, "Roadmap on silicon photonics," *J. Opt.*, vol. 18, no. 7, 2016, Art. no. 073003.
[3] S. Assefa, W. M. Green, A. Rylyakov, C. Schow, F. Horst, and Y. Vlasov, "CMOS integrated nanophotonics: Enabling technology for exascale computing systems," in *Proc. Opt. Fiber Commun. Conf., OSA Tech. Digest (CD)*, 2011, Paper OMM6.
[4] B. Jalali and A. Mahjoubfar, "Tailoring wideband signals with a photonic hardware accelerator," in *Proc. IEEE*, vol. 103, no. 7, pp. 1071–1086, Jul. 2015.
[5] C. A. Thraskias *et al.*, "Survey of photonic and plasmonic interconnect technologies for intra-data center and high-performance computing communications," *IEEE Commun. Surv. Tut.*, vol. 20, no. 4, pp. 2758–2783, Oct.–Dec. 2018.
[6] G. Van der Sande, D. Brunner, and M. C. Soriano, "Advances in photonic reservoir computing," *Nanophotonics*, vol. 6, no. 3, pp. 561–576, 2017.
[7] M. Born, and E. Wolf, "Elements of the theory of diffraction" in *Principles of Optics*, 7th (expanded) ed. Cambridge, U. K.: Cambridge University Press, 1999, ch. 8, pp. 465–472.
[8] E. Ozbay, "Plasmonics: merging photonics and electronics at nanoscale dimensions," *Science*, vol. 311, no. 5758, pp. 189–193, 2006.
[9] R. Zia, J. A. Schuller, A. Chandran, and M. L. Brongersma, "Plasmonics: the next chip-scale technology," *Mater. Today*, vol. 9, no. 7-8, pp. 20–27, 2006.
[10] D. Gramotnev and S. Bozhevolnyi, "Plasmonics beyond the diffraction limit," *Nat. Photon.*, vol. 4, no. 2, pp. 83–91, 2010.

[11] M. I. Stockman *et al.*, "Roadmap on plasmonics," *J. Opt.*, vol. 20, no. 4, 2018, Art. no. 043001.

[12] G. Dabos *et al.*, "CMOS plasmonics in WDM data transmission: 200 Gb/s (8 × 25 Gb/s) transmission over aluminum plasmonic waveguides," *Opt. Express*, vol. 26, no. 10, pp. 12469–12478, 2018.

[13] J. Du and J. Wang, "Design and fabrication of hybrid SPP waveguides for ultrahigh-bandwidth low-penalty terabit-scale data transmission," *Opt. Express*, vol. 25, no. 24, pp. 30124–30134, 2017.

[14] D. Y. Fedyanin, D. I. Yakubovsky, R. V. Kirtaev, and V. S. Volkov, "Ultra-loss CMOS Copper plasmonic waveguides," *Nano Lett.*, vol. 16, no. 1, pp. 362–366, 2016.

[15] H.-R. Park, J.-M. Park, M.-S. Kim, and M.-H. Lee, "A waveguide-typed plasmonic mode converter," *Opt. Express*, vol. 20, no. 17, pp. 18636–18645, 2012.

[16] M. Ono *et al.*, "Deep-subwavelength plasmonic mode converter with large size reduction for Si-wire waveguide," *Optica*, vol. 3, no. 9, pp. 999–1005, 2016.

[17] D. H. Lee and M.-H. Lee, "Gapped surface plasmon polariton waveguides for plasmonic signal modulation applications," *J. Nanosci. Nanotechnol.*, vol. 15, no. 10, pp. 7679–7684, 2015.

[18] D. H. Lee and M.-H. Lee, "Straight long-range surface plasmon polariton waveguides with a gap," *J. Nanosci. Nanotechnol.*, vol. 19, no. 10, pp. 6106–6111, 2019.

[19] D. H. Lee and M.-H. Lee, "Efficient experimental design of a long-range gapped surface plasmon polariton waveguide for plasmonic modulation applications," *IEEE Photon. J.*, vol. 11, no. 1, pp. 1–10, Feb. 2019, Art. no. 4800310.

[20] T. Liu *et al.*, "Transmission of long-range surface plasmon-polaritons across gap in Au waveguide," *J. Opt.*, vol. 18, no. 1, 2016, Art. no. 015006.

[21] ChemOptics Inc.. [Online]. Available: http://www.chemoptics.co.kr

[22] D. F. Edwards and H. R. Philipp, *Handbook of Optical Constants of Solids*, Cambridge, MA, USA: Academic Press, 1985.

[23] D. H. Lee, "Novel nano plasmonic waveguides for compatible plasmon and photon based circuits," Ph.D. dissertation, Dept. Elect. Comput. Eng., Sungkyunkwan Univ., 2019.

[24] D. Sarid, "Long-range surface-plasma waves on very thin metal films," *Phys. Rev. Lett.*, vol. 47, no. 26, pp. 1927–1930, 1981.